

## Recent results and highlights from the CHIMERA Collaboration

E. DE FILIPPO<sup>(1)</sup>(\*), P. RUSSOTTO<sup>(2)</sup>, L. ACOSTA<sup>(3)</sup>(<sup>8</sup>), A. BARBON<sup>(4)</sup>(<sup>1</sup>),  
G. CARDELLA<sup>(1)</sup>, A. CASTOLDI<sup>(5)</sup>(<sup>6</sup>), G. D'AGATA<sup>(4)</sup>(<sup>1</sup>), E. GERACI<sup>(4)</sup>(<sup>1</sup>),  
B. GNOFFO<sup>(4)</sup>(<sup>1</sup>), C. GUAZZONI<sup>(5)</sup>(<sup>6</sup>), C. MAIOLINO<sup>(2)</sup>, N. S. MARTORANA<sup>(1)</sup>,  
A. PAGANO<sup>(1)</sup>, E. V. PAGANO<sup>(2)</sup>, M. PAPA<sup>(1)</sup>, S. PIRRONE<sup>(1)</sup>, G. POLITI<sup>(4)</sup>(<sup>1</sup>),  
L. QUATTROCCHI<sup>(7)</sup>, F. RISITANO<sup>(7)</sup>(<sup>1</sup>), F. RIZZO<sup>(4)</sup>(<sup>2</sup>), G. SACCÀ<sup>(1)</sup>,  
G. SANTAGATI<sup>(1)</sup>, M. TRIMARCHI<sup>(7)</sup>(<sup>1</sup>) and C. ZAGAMI<sup>(4)</sup>(<sup>2</sup>)

<sup>(1)</sup> INFN, Sezione di Catania - Catania, Italy

<sup>(2)</sup> INFN, Laboratori Nazionali del Sud - Catania, Italy

<sup>(3)</sup> Instituto de Fisica, Universidad Nacional Autónoma de Mexico - Mexico City, Mexico

<sup>(4)</sup> Dip. Fisica e Astronomia, University of Catania - Catania, Italy

<sup>(5)</sup> Dip. di Elettronica, Informazione e Bioingegneria, Politecnico di Milano - Milano, Italy

<sup>(6)</sup> INFN, Sezione di Milano - Milano, Italy

<sup>(7)</sup> Dipartimento di Scienze MITF, University of Messina - Messina, Italy

<sup>(8)</sup> Instituto de Estructura de la Materia, CSIC - Madrid, Spain

received 26 November 2024

**Summary.** — The CHIMERA Collaboration uses three main devices in its experimental activities: the CHIMERA  $4\pi$  detector, the FARCOS correlator (Femtoscope Array for Correlation and Spectroscopy) and the new NARCOS plastic scintillators array prototype for neutrons and light charged particles detection. We discuss two recent examples of physics results obtained with these devices: the first one will focus on the AsyEos-II experiment that studies the EoS (Equation-of-State) of neutron rich matter at high baryon densities. The AsyEos-II experiment will be realized in 2025 at GSI/FAIR and it proposes to probe the EoS at densities around  $2\rho_0$  in Au+Au collisions and beam incident energies from 250 to 800 MeV/A. The second one, in the Fermi energy regime, studies dynamical emission of particles at 20 MeV/A beam energy as a function of projectile and target isospin (CHIFAR experiment). Contributions of the CHIMERA Collaboration for the diagnostic and tagging system of the FraISE facility at LNS based on SiC (Silicon Carbide) technology and recent advances of the NARCOS array project will be briefly discussed.

### 1. – Introduction

This article presents a selected view of the most recent and in progress activities of the CHIMERA Collaboration, generally mainly devoted to the physics of heavy-ion collisions from Fermi to relativistic energies with stable or radioactive ion beams, thus involving both nuclear dynamics (fusion, fission, neck emission, isospin diffusion [1-4],

(\*) Corresponding author. E-mail: defilippo@ct.infn.it

isospin equilibration and dipolar degree of freedom [5, 6]) and nuclear structure studies (population and decay of Hoyle and excited states in  $^{12}\text{C}$  related to the understanding the  $^{12}\text{C}$  synthesis in the universe [7, 8], pygmy resonances [9], clustering states in neutron rich nuclei [10-12]). On the other side, traditionally, our collaboration is constantly involved in the development of new detection devices and advances in detection and data analysis technologies [13], mainly connected with the development of high-intensity radioactive beams at INFN-LNS [14] and in other laboratories worldwide. In the following, this paper will describe i) the status of the AsyEos-II experiment, to be realized at GSI/FAIR in March 2025, ii) the status of the CHIFAR experiment, studying dynamical emission of particles at 20 MeV/A beam energy as a function of projectile and target isospin by using the CHIMERA multidetector coupled to 10 telescopes of the FARCOS array [15], iii) the status of the NARCOS (Neutron ARray for CORrelation Studies) prototype for neutrons and charged particles detection [16] and of the SiC array for diagnostic and tagging system in the FraISE facility [17]. For these last two items and some of the physical cases described above more detailed presentations are included in specific contributions to the present volume. Finally, some perspectives for future developments are outlined.

## 2. – The AsyEos-II experiment at GSI/FAIR

Heavy-ion collisions offer the unique opportunity to study the EoS of nuclear matter in a large range of baryonic densities, around the saturation one  $\rho_0$ , and of isospin asymmetry  $\delta = (\rho_n - \rho_p)/\rho$ , where  $n$  and  $p$  refer to neutrons and protons and  $\rho$  is the total density. In asymmetric nuclear matter the EoS can be approximated as a sum of the energy per nucleon for the symmetric nuclear matter  $E(\rho, \delta = 0)$  and the symmetry energy term  $E_{sym}(\rho)$ :  $E(\rho, \delta) = E(\rho, \delta = 0) + E_{sym}(\rho)\delta^2$ . The symmetry energy term can be expanded around its value at nuclear saturation density:

$$(1) \quad E_{sym}(\rho) = E_{sym,0} + \frac{L}{3} \left( \frac{\rho - \rho_0}{\rho_0} \right) + \frac{K_{sym}}{18} \left( \frac{\rho - \rho_0}{\rho_0} \right)^2 + \dots,$$

where  $E_{sym,0} = S_0$ ,  $L$ , and  $K_{sym}$  are respectively the value of symmetry energy, the slope (related to neutron pressure) and the curvature parameter at  $\rho_0$ . Constraining the asymmetry term of the EoS is important, amongst other reasons, for its strict connection with multi-messenger astronomy related to astrophysical observations such as mass and radius of neutron stars, mergers of compact binary stars and tidal deformability in gravitation wave events (related to the radius of a neutron star) detected by LIGO/Virgo Collaboration [18], precise measurements of the neutron stars radius by X-rays detection from spatial observatories (NICER) [19-21]. The EoS and the asymmetry term of EoS at supra-saturation density govern the main properties of a neutron star and, in particular, the mass and radii relation. On the other hand,  $E_{sym}(\rho)$  is fundamental to study the nuclei masses, drip lines, collective excitations in nuclei, dynamics of heavy-ion collisions and particles flow from Fermi to relativistic energies [22, 23]. Astrophysical observations and terrestrial laboratory data, coming mainly from heavy-ion collisions measurements, can be combined to improve the constraints of dense matter in neutron stars [24, 25]. Anyway, there are only sparse experimental data, by using relativistic heavy-ion collisions, probing the EoS of asymmetric matter at supra-saturation densities: among them, the FOPI data on charged pions ratio [26], the FOPI-LAND data [27], the AsyEos data (elliptic flows of neutrons and hydrogen nuclei) [28], the S $\pi$ RIT data (charged pion ratio) [29], the HADES data on collective flow  $v_n$  coefficients of order 1–4 [30].

The AsyEos experiment, by using as main observable the elliptic flow  $v_2$  ratio of neutrons and charged particles [28], probed the isospin-dependent component (asymmetry term) of the EoS at densities around  $1-2\rho_0$  in Au+Au collisions at 400 MeV/A. The elliptic flow  $v_2$  is a measure of the “squeeze-out” of the nuclear matter out of the reaction plane and it develops at relativistic energies from the pressure gradient between the highest density region and the surrounding ones at lower densities (spectators) [31].  $v_2$  is defined by the second moment of the Fourier expansion of the azimuthal angle distribution of the emitted particles with respect to the reaction plane. The robustness of the  $v_2$  ratio observable in probing the asymmetry part of the EoS has been shown for example in UrQMD calculations [27] where, for the  $^{197}\text{Au}+^{197}\text{Au}$  at 400 MeV/A, the predictions of the elliptic flow of neutrons, protons and hydrogen yields are compared for two choices of the stiffness of density dependence of the symmetry energy, described by a power-law  $E_{\text{sym}}(\rho) = 22(\rho/\rho_0)^\gamma + 12(\rho/\rho_0)^{2/3}$  MeV in the model. It results in a large neutron squeeze-out in the stiff case ( $\gamma = 1.5$ ) with respect to the soft one ( $\gamma = 0.5$ ), while proton and hydrogen flows depend weakly on  $\gamma$  variations. In the AsyEos experiment performed at GSI [28] data from the elliptic flow ratio of neutrons and hydrogens  $v_2^n/v_2^h$  as a function of their transverse momentum were compared with the UrQMD model in order to probe the asymmetry term of the EoS. The value of  $L$  obtained was  $L = 72 \pm 13$  MeV for  $E_{\text{sym}}(\rho_0) = 34$  MeV. This result is displayed in fig. 1 (left panel) where the symmetry energy is shown as a function of density for AsyEos (orange band) and old FOPI-LAND [27] (yellow band) data. A large review of this experiment in the context of studies on EoS mainly carried out at GSI and discussion of different theoretical approaches to the data can be found in ref. [32]. Recently, a Bayesian inference technique has been used [25] combining astrophysical observations with data from heavy ion collisions (AsyEos and FOPI data) and results of microscopic interactions from chiral effective field theory ( $\chi$ EFT). The starting point of the calculation are  $\chi$ EFT interactions, used as a “theoretical prior”, producing the largest uncertainties for the EoS at high densities. The uncertainties are reduced adding data from astrophysical observations and heavy-ion collisions (HIC) data. Results are summarized in fig. 1 (right panel) where the

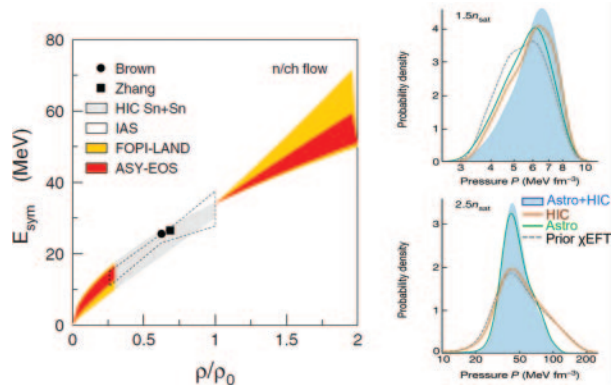


Fig. 1. – Left panel: constraint to the EoS symmetry term deduced from the ASYEOS experiment (red band) and FOPI-LAND experiment (yellow) compared to low density results (see refs. [28,32] for details). Right panel: distribution of the pressure  $P$  at  $1.5\rho_0$  (upper) and  $2.5\rho_0$  (bottom) densities, in a Bayesian analysis for different contributions indicated in the labels (see text). Adapted from ref. [25].

distribution of pressure of nuclear matter is shown at  $1.5\rho_0$  (top) and  $2.5\rho_0$  (bottom). The inclusion of HIC data is significant mainly at  $1.5\rho_0$  and produces a stiffness of the EoS giving as result a radius of  $12 \pm 0.78$  km at  $1.4M_\odot$  neutron star mass within 95% credible interval. At  $2.5\rho_0$  HIC results are scarce or missing and show less sensitivity with respect to astrophysical observations.

The AsyEos-II experiment proposes to extend the knowledge of the symmetry energy to higher densities near  $2\rho_0$  (by using incident energies from 250 up to 800 MeV/A) and to improve the measurement precision with respect to the previous one. The first goal can be achieved in various ways: i) the usage of the highest energy beam at 800 MeV/A should increase the central baryon density reached as predicted by transport models [33, 34]; indeed simulations with UrQMD model on Au+Au collisions from 0.250 to 1 GeV/A (see fig. 24 of ref. [32]) shows that the sensitivity of the  $v_2^n/v_2^p$  elliptic flow ratio to the symmetry energy is maintained, and it slightly decreases when going to the highest beam energy (1 GeV/A). ii) Predictions of the TuQMD model [35] show that  $v_2^n/v_2^p$  (p: protons) and  $v_2^n/v_2^h$  (h:  $Z = 1$  isotopes) elliptic flow ratios probe different density regimes, on average around  $1.4\text{--}1.5\rho_0$  and  $1.0\text{--}1.1\rho_0$ , respectively, for Au+Au at 400 MeV/A, thus a measure of the n/p ratio with respect to n/h ratio (as in the AsyEos experiment) will probe higher densities than previously done. iii) The same model predictions show the feasibility of constraining simultaneously the slope  $L$  and the curvature parameter  $K_{sym}$  of the symmetry energy using elliptic flow data. The model predicts the maximum sensitivity for the  $K_{sym}$  determination around 250 MeV/A incident energy, that is one of the beam energies planned by the AsyEos-II experiment. The second goal is achieved by using an innovative and powerful detector ensemble that is shown in fig. 2 in cave C at GSI/FAIR within the R<sup>3</sup>B (Reactions with Relativistic Radioactive Beams) Collaboration. KRAB is a new detector [32], developed at IFJ PAN, Krakow, constituted by 5 rings of  $4 \times 4$  mm<sup>2</sup> fast scintillating fibers (BCF-10) with readout by SiPMs, for a total of 736 channels, placed around the target. It will provide a fast trigger based on multiplicity, charged particles azimuthal distributions for event-by-event reaction plane reconstruction and it allows for discrimination of off-target (in air) reactions. Amongst the R<sup>3</sup>B Collaboration devices, the NeuLAND detector [36] for high efficiency neutron and H isotopes detection and two frames of the time-of-flight ToFD, made by plastic scintillator paddles [37], will be used. The first ToFD frame in order to measure particles velocity and charge at very forward angles, and the second one acting as a charged particles veto for the NeuLAND detector. Finally, four rings (ring 3 to 6) of the CHIMERA array (mainly around 400 CsI(Tl) scintillators) will improve the determination of the impact parameter and reaction plane orientation of the events. The AsyEos-II experiment (s122) will measure at 3 different energies (250, 400 and 800 MeV/A) of Au beam, where 400 MeV/A is the reference energy related to the previous results.

In March 2024 the new KRAB detector and the coupling of the acquisition systems (DAQ) of the different detectors were commissioned under beam at GSI/FAIR. Gold beams of 400 and 800 MeV/A were used. The Chimera detector was “emulated” by using a two stage DSSSD telescope (from FARCOS array), both  $32 \times 32$  strips, 1500  $\mu$ m thick, placed between 8 and 15 degrees on one side with respect to KRAB. The ToFD array was also present at forward angles. The plastic scintillator LOS start detector (part of R<sup>3</sup>B setup) gave the start signal for time-of-flight measurements. In R<sup>3</sup>B setup each DAQ node (related to a given detector) uses timestamp clock references, that are synchronized. The White-Rabbit (WR) protocol is generally used. In the CHIMERA node a VME WR receiver, VETAR2, operating at 125 MHz, 64 bit words length, is connected by optical fiber to a high-precision subnanosecond timing WR switch and synchronized with all

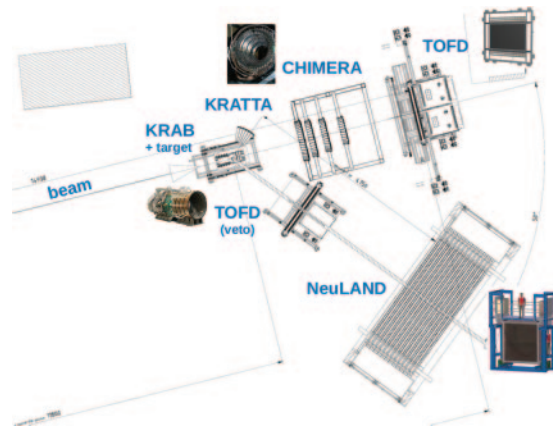


Fig. 2. – Schematic setup of the planned AsyEos-II experiment in cave C at GSI/FAIR.

DAQ nodes. In s122 beam test CHIMERA WR timestamp synchronization with the master DAQ performed well with a good stability and a time jitter limited to  $\approx 3$  ns. Time sorted data are grouped in the same physical event by using a time window ( $< 4 \mu\text{s}$ ) based on timestamp. In order to have on-line synchronization check, the master trigger is sent to all subsystems as a randomly variable width. The recorded width values are plotted event by event for stitched events with the corresponding data in master DAQ. Figure 3 (left) shows results of this “synch-check” procedure. The diagonal line in the figure indicates correlated events.

KRAB commissioning gave also positive results. Tests concerned the electronic cross-talks, investigation on  $\delta$ -electron production along the beam path, reaction plane dispersion and the possibility of discrimination of the off-target events (reaction of beam with air). The test allowed to keep the electronic cross-talks between the adjacent wires on an a level around 1% per event for cross-talks with multiplicity 4. Off-line reaction plane re-construction was also tested both standalone and also requiring a coincidence with the DSSSD telescope simulating CHIMERA. Results are presented in fig. 3 (right), where the effect on the spectra distribution of an increasing multiplicity of particles detected in DSSSD in coincidence with KRAB is evident.

The experiment s122 is scheduled for March 2025 and preparation is in progress.

### 3. – Status of the CHIFAR experiment

The CHIFAR experiment studies primarily the competition between reaction mechanisms in the Intermediate Mass Fragments (IMF) emission near the low boundary of the Fermi energy domain (20 MeV/A), following the studies previously conducted with CHIMERA detector in experiments at 35 MeV/A beam energy. In particular, in one of the last works, the IMFs production probability was studied from projectile-like break-up in non-central reactions in collisions of  $^{124}\text{Xe}$ ,  $^{124}\text{Sn}$  projectiles with targets of  $^{64}\text{Ni}$  and  $^{64}\text{Zn}$  at energy of 35 MeV/A [3]. Cross-sections for statistical and dynamical emission processes were determined and compared. We found that, for these isobaric systems dynamical emission is favored by an increase of both projectile and target  $N/Z$  isospin and it reaches the maximum for the most neutron rich system  $^{124}\text{Sn} + ^{64}\text{Ni}$ . In the CHIFAR experiment, reactions of  $^{124}\text{Xe}$ ,  $^{124}\text{Sn}$  and  $^{112}\text{Sn}$  at 20 MeV/A delivered by the Superconducting Cyclotron (CS) of INFN-LNS impinged on targets of  $^{64}\text{Ni}$ ,  $^{64}\text{Zn}$  and  $^{58}\text{Ni}$ .

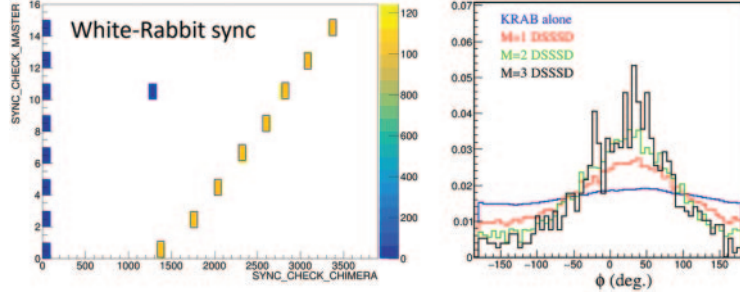


Fig. 3. – Commissioning experiment s122/2024. Left panel: on-line synchronization check between CHIMERA data and master DAQ. Right panel: Raw reaction plane determination in KRAB requiring coincidence with different charged particle multiplicities detected in strip detectors DSSSD.

The CHIMERA  $4\pi$  detector was coupled to 10 telescopes of the FARCOS array [15], in a ring-like setup covering polar angles between 16 and 30 degrees. Results relative to standalone data in FARCOS are presented elsewhere in this volume [38].

Some preliminary results of the CHIFAR experiment were presented in [39]. Here we only show some recent advances in data analysis. Due to the combination of relatively low incident energy and heavy masses of projectile and fragments, most of the emitted particles are stopped in the first silicon detector stage ( $\sim 300 \mu\text{m}$  thick) of the CHIMERA telescopes. We developed a semi-automatic procedure for mass and velocity determination in silicon detectors by means of the  $E$ - $ToF$  method, where  $ToF$  is the time-of-flight of the particle with respect to the CS radio-frequency signal and  $E$  its energy. This procedure takes into account also nonlinear effects induced by electronic walk and plasma delay in silicon. The uncertainty in mass assignment varies from 7% for light fragments to 15–20% for masses  $A \gtrsim 80$ . This identification technique is presented in ref. [40] and was largely applied in CHIFAR data analysis.

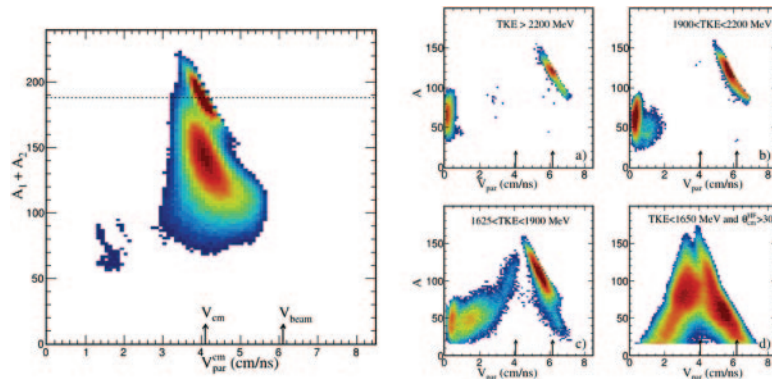


Fig. 4. – Left panel: for the  $^{124}\text{Sn}+^{64}\text{Ni}$  reaction and  $M_{IMF} = 2$  IMF multiplicity the sum of their masses  $A_1 + A_2$  ( $A_i > 16$ ) is reported as a function of the component along the beam axis of c.m. velocity. Right panel: correlation between the mass  $A$  of the fragments and their parallel velocity  $V_{par}$  for different gates on TKE (lower values of TKE indicate more dissipative reactions). Arrows indicate beam and c.m. velocities, respectively.

The starting point of the analysis presented here is the selection of events with  $M_{IMF} = 2$  and masses  $A_i > 16$ . Figure 4 (left panel) shows the sum of the two masses as a function of their c.m. velocity component along the beam axis. The two loci clearly seen in the figure along the c.m. velocity are respectively the region of complete detected events ( $A_1 + A_2 \approx 188$ ) and the region around  $A_1 + A_2 \approx 124$  where only the projectile-like fragments (PLF) were detected. Both these two regions were considered in order to construct the total kinetic energy  $TKE = \sum_i E_{kin}^i$  of the fragments, taken as an index of the degree of dissipation in the reaction. Figure 4 (right panel) shows, for different selections of the TKE, the correlation between mass  $A$  and parallel velocity  $V_{par}$  of the fragments. We clearly see the evolution from quasi-elastic collisions (panel (a)) to deep inelastic collisions (panel (b), (c)) and finally, for the most dissipative collisions (panel (d)) to fusion-fission (FF) reactions, where the two branches of fission products from fusion are clearly recognized. In this last case, a further condition to enforce the selection of FF reactions was used, imposing that  $\Theta_{c.m.}^{HF} > 30^\circ$ , where  $\Theta_{c.m.}^{HF}$  is the polar deflection angle of the heavier fragment (HF) in the c.m. of the two particles. This last selection comes from the inspection of the bi-dimensional plot  $TKE - \Theta_{c.m.}^{HF}$  (Wilczyński plot) where angles greater than  $30^\circ$  further select the most dissipative reactions.

It is clear from fig. 4 that at the incident energy of 20 MeV/A there is an increase of complexity and mixing of different reaction mechanisms populating the same loci (for example fragments from projectile-like fission and fragments from fusion-fission reactions) with respect to the same reactions previously studied at higher incident energy (35 MeV/A) [2, 3].

The cross-section for FF mechanism, corrected for detector response, has been measured for the systems indicated in fig. 5 and is shown as red histograms. We observe a greater cross-section for reactions induced by the neutron rich  $^{124}\text{Sn}$  projectile with a weaker dependence on target neutron richness. In fact, for the neutron poor systems complete fusion should be partially inhibited because a compound nucleus with mass around  $A \approx 180$  corresponds to proton rich nuclei further away from the stability valley. We compared results by using the phenomenological event generator HIPSE [41] with statistical deexcitation simulated by the code SIMON (embedded in HIPSE) or by the GEMINI code [42]. The data behaviour is generally well reproduced, if we look at the isospin dependence of the FF cross-section, but the experimental cross-sections are underestimated by the calculations. However, experimental data selection is still preliminary and contaminations from projectile break-up or other processes in the FF cross-section are possible at this level of data analysis.

One of the main goals of our analysis is the study of competition of statistical and dynamical fission of the PLF as a function of the entrance channel isospin content [2, 3, 43-45]. The complex selection of the PLF break-up channel will not be detailed here. The main ingredient is the requirement of coincidence with a detected target-like (TLF) fragment in events with total multiplicity greater than 2. Called  $A^H$  and  $A^L$ , respectively, the heavy and light fragments of the PLF break-up we used the further conditions that  $103 \leq A^H + A^L \leq 139$  and their relative velocity within 30% of the one expected for Coulomb repulsion in a equilibrated break-up (Viola systematics). Figure 6 shows the normalized yields in  $\cos(\theta_{prox})$  distributions for the two reactions  $^{124}\text{Sn} + ^{64}\text{Ni}$  (empty circles) and  $^{112}\text{Sn} + ^{58}\text{Ni}$  (black circles) as a function of the PLF mass asymmetry  $A^H/A^L$  from the most asymmetric break-up (panel (a)) to the most symmetric ones (panel (d)).  $\theta_{prox}$  is the angle between the relative velocity  $V_{rel}$  axis, oriented from  $A^L$  to  $A^H$  of the primary PLF break-up, and the PLF recoil velocity in the center of

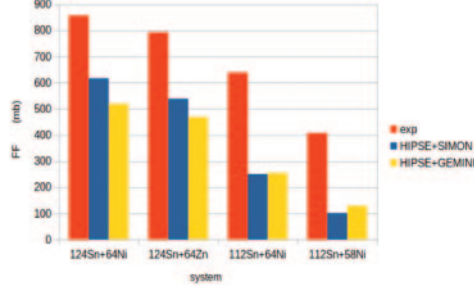


Fig. 5. – Experimental fusion-fission cross-section (red histograms) for the studied systems, corrected for detector response compared with HIPSE+SIMON (blue) and HIPSE+GEMINI (yellow) calculations.

mass. The weights of the dynamical and statistical components are disentangled by using the  $\cos(\theta_{prox})$  distribution following methods described in refs. [2,3] for the reactions at 35 MeV/A. Dynamical emission is evidenced by the strong peak at  $\cos(\theta_{prox}) \approx 1$ , in particular for the most asymmetric break-up and the forward-backward asymmetry in the  $V_{par}$ - $V_{per}$  plots shown as insets in the figure for the  $A^L$  fragment. In fact, the light fragment is backward emitted in the reference frame of the primary PLF (conversely, statistical emission leads to an isotropic distribution).

For the four systems studied at 20 MeV/A the cross-sections for dynamical and statistical break-up were extracted after correcting for detection efficiency. Figure 7 shows preliminary results for dynamical (red circles) and statistical emission (blue triangles).

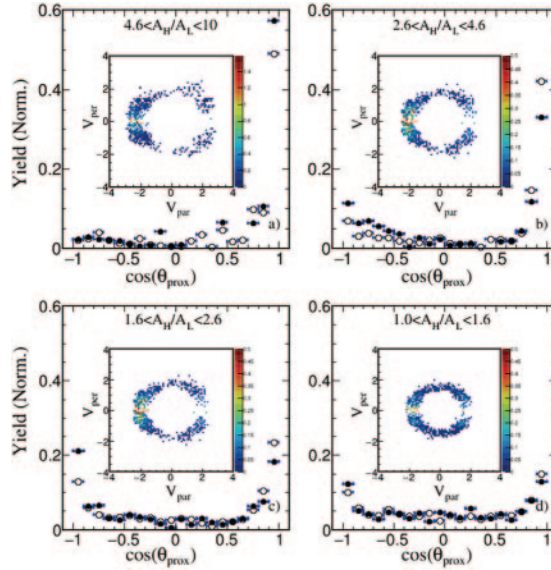


Fig. 6. – Normalized  $\cos(\theta_{prox})$  distributions for different selections of PLF break-up asymmetry, from more asymmetric (a) to symmetric one (d) for the two reactions  $^{124}\text{Sn}+^{64}\text{Ni}$  (empty circles) and  $^{112}\text{Sn}+^{58}\text{Ni}$  (black circles). The insets show for the reaction  $^{124}\text{Sn}+^{64}\text{Ni}$  the Galilean invariant cross-section for  $A^L$  in the reference frame of the PLF.

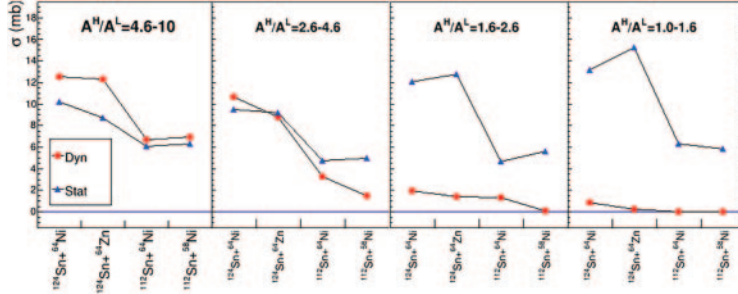


Fig. 7. – Cross-sections for dynamical (red points) and statistical (blue triangles) break-up as a function of the mass asymmetry  $A^H/A^L$  and for the four systems studied at 20 MeV/A.

The most interesting result is the persistence of the same effect already observed at 35 MeV/A: an increase of the cross-section associated to dynamical break-up with the neutron richness of both the projectile and target. Conversely, with respect to the results found at 35 MeV/A, the statistic emission shows also a dependence on isospin of the entrance channel, in particular for the most symmetric break-up.

#### 4. – Brief highlights on the NARCOS and SiC detector array projects

The starting trigger for the project of these new devices was the recent effort in many laboratories worldwide for the construction of new facilities for high-intensity radioactive ion beams (RIBs), including the FraISE project at INFN-LNS [14,46]. The NARCOS prototype is an array of 64 plastic scintillator detectors (EJ-276G family) whose elementary cell has a dimension of  $3 \times 3 \times 3 \text{ cm}^3$ , arranged in a cubic geometry and individually read by Silicon Photomultiplier (SiPM) [16]. The array detects  $\gamma$ -rays, neutrons and light charged particles. Particle discrimination is done by using pulse shape discrimination and time-of-flight measurements. It performs high angular and energy resolutions, with good detection efficiency for neutrons (larger than 50%). The final prototype is expected to have 64 elementary cells in 16 clusters (each cluster constituted by 4 consecutive elementary cells). The most recent achievements in the project were: i) the experimental characterization of discrimination capabilities of EJ-276G (green light) [47]; ii) a detailed study of the efficiency and cross-talk probability of the device in various configuration by GEANT4 simulations [48]; iii) the construction of a SiPM read-out electronic motherboard for a square matrix of 9 ( $3 \times 3$ ) plastic scintillators; iv) the CROSSTEST experiment, performed in November 2023 at the CN electrostatic accelerator of INFN-LNL. This experiment proposes to experimentally evaluate the crosstalk probability in the device among the elementary detection cells at low neutron energy ( $E_n < 5 \text{ MeV}$ ) and in various geometrical configurations.

A critical point for high-intensity radioactive ion beams facilities, like FraISE, is monitoring and tuning the transport of high-quality beams. Indeed tagging devices selecting different RIBs are needed. Within this framework, there is a notable interest in employing Silicon Carbide (SiC) technology as tagging and diagnostics detection systems for example for its radiation hardness and good sub-nanoseconds timing properties. In this framework, an array of SiC detectors is being developed [17]. The final system consists of an array of SiC detection pads with an area of  $3 \times 5 \text{ mm}^2$  and a thickness of  $180 \mu\text{m}$  ( $160 \mu\text{m}$  active thickness). Arranging several pads in rows and columns allows to cover an area of  $\approx 60 \times 30 \text{ mm}^2$ . This segmentation will be able to intercept the RIBs in the

high-dispersion point, to extract the beam profile, and to sustain intensity of  $\approx 10^7$  pps. The most recent achievements in the project were: i) characterization of  $2 \times 2$  monolithic SiC detector with a Mesytec preamplifier and a CAEN digitizer DT5742 with radioactive sources and with ion beams; ii) the development of a fast dedicated front-end electronics based on charge pre-amplifier board [49, 50]; iii) development of innovative methods for studying timing properties of the digitized signal of the SiC detector by  $\alpha$  mixed radioactive sources impinging in two adjacent pads. A detailed presentation of these topics is included in specific contributions to the present volume [51, 52].

## 5. – Conclusions and new opportunities

We have summarized some aspects of the most recent scientific activity of the CHIMERA Collaboration. The first focus was in the AsyEos-II experiment where we have illustrated the relevance to determine the symmetry energy in the region of supra-saturation densities around  $2\rho_0$ . In the context of the multi-messenger astronomy new results could be relevant for simulations of astrophysical objects and processes for which constraints from other sources are relatively scarce and for refinements on transport and microscopic models describing the EoS of nuclear matter [53]. The second focus was on CHIFAR experiment that has reached an advanced phase of data analysis. Both data at 20 and 35 MeV/A on projectile-like break-up confirm the dependence of IMF dynamical emission from the  $N/Z$  isospin of the entrance channel. We plan the comparison of both sets of data with transport model simulations in order to deeply investigate the role of isospin in the dynamical instabilities in this process. Indeed the merging of FARCOS and CHIMERA data (not yet done) will enrich the experimental datasets available. Clearly, a turning point in heavy-ion collisions and studies to probe the EoS of nuclear matter, from low energies to relativistic regime, is the use of high-intensity radioactive beams worldwide. The project of ancillary and portable devices as FARCOS or NARCOS goes also in this direction. Recently, ideas for new projects and experiments, including contributions from CHIMERA Collaboration for nuclear structure and nuclear dynamics, were collected in two white papers discussing mid-term plans for nuclear physics at FraISE@LNS [14] and SPES@LNL [54]. CHIMERA Collaboration is also involved in a scientific initiative together with INDRA/FAZIA group for experimental campaigns at MSU-FRIB exploiting high-intensity beams such as  $^{54}\text{Ni}$ ,  $^{70}\text{Ni}$ ,  $^{104}\text{Sn}$ ,  $^{132}\text{Sn}$ , and for the FRIB400 project.

\* \* \*

This work has been supported by the European Community Horizon 2020 – research and innovation programme, contract STRONG-2020 No. 824093.

## REFERENCES

- [1] DE FILIPPO E. and PAGANO A., *Eur. Phys. J. A*, **50** (2014) 32.
- [2] RUSSOTTO P. *et al.*, *Phys. Rev. C*, **91** (2015) 014610.
- [3] RUSSOTTO P. *et al.*, *Eur. Phys. J. A*, **56** (2020) 12.
- [4] PAGANO A., DE FILIPPO E., GERACI E. *et al.*, *Eur. Phys. J. A*, **56** (2020) 102.
- [5] PAPA M. *et al.*, *Phys. Rev. C*, **91** (2015) 041601(R).
- [6] PAPA M. *et al.*, *EPJ Web of Conferences*, **301** (2024) 02007.
- [7] CARDELLA G. *et al.*, *Phys. Rev. C*, **104** (2021) 064315.
- [8] CARDELLA G. *et al.*, *Nuc. Phys. A*, **1020** (2022) 122395.

- [9] MARTORANA N. S. *et al.*, *Phys. Lett. B*, **782** (2018) 112.
- [10] RISITANO F. *et al.*, *Nuovo Cimento C*, **47** (2024) 43.
- [11] RISITANO F. *et al.*, *EPJ Web of Conferences*, **311** (2024) 00031.
- [12] DELL'AQUILA D. *et al.*, *Phys. Rev. C*, **93** (2016) 024611.
- [13] CARDELLA G. *et al.*, *Nucl. Instrum Methods A*, **1069** (2024) 169961.
- [14] AGODI C. *et al.*, *Eur. Phys. J. Plus*, **138** (2023) 1038.
- [15] PAGANO E. V. *et al.*, *EPJ Web of Conferences*, **117** (2016) 10008.
- [16] PAGANO E. V. *et al.*, *Front. Phys.*, **10** (2022).
- [17] MARTORANA N. S. *et al.*, *Nuovo Cimento C*, **47** (2024) 56.
- [18] ABBOTT B. P. *et al.*, *Phys. Rev. Lett.*, **121** (2018) 161101.
- [19] RILEY T. E. *et al.*, *Astron J. Lett.*, **918** (2021) 27.
- [20] WATTS A. *et al.*, *Rev. Mod. Phys.*, **88** (2016) 021001.
- [21] LEGRED I. *et al.*, *Phys. Rev. D*, **104** (2021) 063003.
- [22] HOROWITZ C. J. *et al.*, *J. Phys. G: Nucl. Part. Phys.*, **41** (2014) 093001.
- [23] SORENSEN A. *et al.*, *Progr. Part. Nucl. Phys.*, **134** (2024) 104080.
- [24] TSANG C. Y. *et al.*, *Nat. Astron.*, **8** (2024) 328.
- [25] HUTH S. *et al.*, *Nature*, **606** (2022) 276.
- [26] XIAO Z., BAO-AN LI *et al.*, *Phys. Rev. Lett.*, **102** (2009) 062502.
- [27] RUSSOTTO P. *et al.*, *Phys. Lett. B*, **697** (2011) 471.
- [28] RUSSOTTO P. *et al.*, *Phys. Rev. C*, **94** (2016) 034608.
- [29] LYNCH W. G. and TSANG M. B., *Phys. Lett. B*, **830** (2022) 137098.
- [30] ADAMCZEWSKI-MUSCH J. *et al.*, *Eur. Phys. J. A*, **59** (2023) 80.
- [31] LE FÉVRE A. *et al.*, *Phys. Rev. C*, **98** (2018) 034901.
- [32] RUSSOTTO P. *et al.*, *Riv. Nuovo Cimento*, **46** (2023) 1.
- [33] BAO-AN LI, *Nucl. Phys. A*, **708** (2002) 365.
- [34] LE FÉVRE A. *et al.*, *Nucl. Phys. A*, **945** (2016) 112.
- [35] COZMA M. D., *Eur. Phys. J. A*, **54** (2018) 40.
- [36] BORETZKY K. *et al.*, *Nucl. Instrum Methods A*, **1014** (2018) 40.
- [37] HEIL M. *et al.*, *Eur. Phys. J. A*, **58** (2022) 248.
- [38] ZAGAMI C. *et al.*, these proceedings.
- [39] RUSSOTTO P. *et al.*, *Nuovo Cimento C*, **45** (2022) 55.
- [40] RUSSOTTO P. *et al.*, *Nucl. Instrum Methods A*, **1056** (2023) 168593.
- [41] LACROIX D., VAN LAUWE A. and DURAND D., *Phys. Rev. C*, **69** (2004) 054604.
- [42] CHARITY R. J., *Phys. Rev. C*, **71** (2005) 044602.
- [43] DE FILIPPO E. *et al.*, *Phys. Rev. C*, **71** (2005) 064604.
- [44] RODRIGUEZ MANSO A. *et al.*, *Phys. Rev. C*, **95** (2017) 044604.
- [45] CIAMPI C. *et al.*, *Phys. Rev. C*, **108** (2023) 054611.
- [46] MARTORANA N. S. *et al.*, *Front. Phys.*, **10** (2022).
- [47] PAGANO E. V. *et al.*, *Nucl. Instrum Methods A*, **1064** (2024) 169425.
- [48] SANTAGATI G. *et al.*, *RAD Conf. Proc.*, **7** (2023) 52.
- [49] CASTOLDI A. *et al.*, *IEEE Trans. Nucl. Sci.*, **70** (2023) 1431.
- [50] ACOSTA L. *et al.*, *2022 IEEE Nuclear Science Symposium and Medical Imaging Conference (NSS/MIC)* (IEEE) 2022, <http://doi.org/10.1109/NSS/MIC44845.2022.10398915>.
- [51] GNOFFO B. *et al.*, these proceedings.
- [52] MARTORANA N. S. *et al.*, these proceedings.
- [53] LE FÉVRE A. *et al.*, *EPJ Web of Conferences*, **290** (2023) 10004.
- [54] BALLAN M. *et al.*, *Eur. Phys. J. Plus*, **138** (2023) 709.